Atom Indonesia

Journal homepage: https://atomindonesia.brin.go.id

Monte Carlo Methods to Simulate the Propagation of the Created Atomic/ Nuclear Particles from Underground Piezoelectric Rocks through the Fractures Before the Earthquakes

A. Bahari*, S. Mohammadi, N. S. Shakib, M. R. Benam, Z. Sajjadi

Department of Physics, Payame Noor University, Tehran 19395-469, Iran.

ARTICLE INFO

Article history:
Received 13 March 2023
Received in revised form 2 November 2023
Accepted 15 November 2023

Keywords:
MCNP
Granite rocks
Earthquake
Particles radiation
Gamma ray
Neutrons
Runaway electrons

ABSTRACT

Until now, many studies have been performed on particle radiations before or during earthquakes (EQs). Neutron, gamma, electron, proton, and ultra-low frequency (ULF) photons are among the particles, detected during EQs. In our previous study, with the help of piezoelectricity relationships and the elastic energy formula, the Monte Carlo N-Particle eXtended (MCNPX) simulation code was applied to find the amount of created atomic/nuclear particles, the dominant interactions; and the energy of the particles for various sizes of quartz and granite blocks. In this study, using the MCNPX simulation code, we have estimated the flux of the particles (created from under-stressed granitic rocks) at different distances from the EQ hypocenter inside the fractures, filled with air, water, and CO_2. It was found that inside a water-filled fracture, the particles do not show the flux far from the EQ hypocenter. However, inside the gases like air and CO_2 with the normal condition density, different types of particles can have a flux far from the source (more than a kilometer) and they might reach themselves to the surface in the case that the EQ hypocenter is very shallow (0-5 km). However, for deep EQs, it seems that the most detected nuclear particles on the surface should pass via the vacuum-filled fractures and reach the surface. Moreover, it was concluded that the higher the density of the fracture's filling fluid, the less distance that the particles can have a flux.

INTRODUCTION

Until now, many studies have been performed on the particle radiations before or during the earthquakes. Guo et al. analyzed the characteristic response of gamma radiation monitoring to seismic activity with the data provided by China EQ Data Center. The gamma radiation monitoring in Changsha indicates that near-field EQ swarm or violent EQ affects the gamma radiation in the aseismic region [1].

Salikhov et al. monitored the radiation background in the near-surface atmosphere and gamma rays, geo-acoustic emission, and temperature in a borehole at 40 m depth in northern Tien Shan. The flux of gamma rays in the borehole varied negligibly between the days before EQs [2].

Tsabaris found that gross γ-ray intensity had increased gradually since 10 days before the earthquake (Itea, 30/3/2019). Strong anomalies were detected at 52 h 20 min and 7 h 20 min before the earthquake, respectively [3].

Maksudov and Zufarov proposed a new method for EQ forecasting, based on simultaneous recording of the intensity of fluxes of low-energy neutrons and charged particles by detectors [4].

Stenkin et al. also observed some anomalies in the dynamics of the neutron flux around the time of the catastrophic earthquakes of magnitude M = 7.8 that happened in Gorkha (Nepal) on 25/04/2015 [5].

Moreover, Picozza et al. analyzed electric field data detected by the DEMETER satellite for high-magnitude earthquakes in Indonesia and Chile

*Corresponding author.
E-mail address: aboozar.bahary@gmail.com
DOI: https://doi.org/10.55981/aij.2024.1311

regions, and they reported perturbations of the electromagnetic field of about 10 mV/m, over the epicenter of EQs. This value measured in space should be reconciled with that measured on ground that is several orders of magnitude higher, but never exceeding 100 V/m over an area of 100-1,000 km around the epicenter [6].

The study of Mansouri Daneshvar and Freund affirms a process, by which tectonic stresses deep in the Earth's crust lead to positive charges at the surface-to-air interface and air ionization, which can trigger atmospheric blocks [7].

Carpinteri et al. showed common cycles between interannual changes in atmospheric CO_2 growth rate and global seismic-moment release with a spectral analysis of the period 1955-2013. They concluded that the crucial stages in the geochemical evolution of the Earth's crust, ocean, and atmosphere could be explained by the assumed low-energy nuclear reactions that are triggered by seismic activity [8].

With the help of piezoelectricity relationships and the elastic energy formula, Bahari et al. applied the Monte Carlo simulation to find the amount of created atomic/nuclear particles, the dominant interactions, and the possible particle energies for various sizes of quartz and granite blocks. They have proved that for the large granite blocks, "photonuclear" interactions from the "Bremsstrahlung gamma ray" photons is the main mechanism for nuclear particle creation when the stress is exerted on a large block due to the runaway electron avalanche. In addition, they have presented some formulas to estimate the quantity and energy of various created particles on a fracture surface when the piezoelectric block is under different uniaxial stress [9].

Fractures are breaks or mechanical discontinuities in rock that consist of two rough surfaces in partial contact. The voids between contacts provide the flow and transport paths through fractured rock. Fractures are intrinsically planes of weakness; slight perturbations in stress can displace the fractures, opening or closing the voids, thus affecting flow and transport. Radioactive gases like Xenon, induced by nuclear blast tests, can seep through fractures to the atmosphere anywhere from within minutes to months [10]. The fracturing enhances the permeability, providing additional fluid transport [11-14].

Fractures might be filled with fluids like air, oil, gas, water, and CO_2. In this situation, the type and state of the fluid (liquid or gas) can make a large difference in the response of the seismic waves [15]. Moore et al. analyzed the impact of air and water circulation in deep open fractures on the subsurface thermal field. They have supposed that the origin of convective fracture flow might be due to the fact that during the winter, air at depth is warmer and lighter than atmospheric air, and the resulting density contrast or pressure difference of the columns drives localized convection cells [16].

In this study, using the MCNPX simulation code, we want to answer the question of how the particles created from under-stressed piezoelectric granitic blocks propagate inside the fractures, filled with fluids like air, water, and CO_2 can reach themselves to the surface. This would be beneficial for understanding the particles' propagation mechanism and to find the flux of the particles at different distances from the EQ hypocenter.

METHODOLOGY

Photonuclear reactions as a result of runaway electron avalanche

Free electrons would accelerate (runaway) in a medium where they gain energy from an electric field. Huge amounts of electric fields can be produced from the piezoelectricity of giant granitic blocks before the EQ happens, due to the mechanical stress applied to the rock mass [9]. Besides, large electric fields inside the thunderstorms can produce accelerated electrons [17].

Such energetic electrons would knock the other atoms' nucleus and electrons layers and produce a shower of other electrons. Depending on the propagated electrons energy, different atomic/nuclear interactions may be expected: ionization and atomic excitation, bremsstrahlung photons, elastic/inelastic scattering, pair production, positron annihilation, photoelectric absorption, Compton scattering, and pair production [17]. For instance, Sarria et al. applied different Monte Carlo codes to model the interaction of runaway electrons with up to 40 MeV energy with atmospheric air to analyze the production of high-energy particles in phenomena like terrestrial gamma-ray flashes (TGFs) [18].

A gamma photon with energy sufficiently large to overcome the nuclear binding energy (about 7 MeV in most nuclides) may result in the emission of nucleons ((γ, n) or (γ, p) reactions), α particles, or other particles. The cross-section for photonuclear reactions exhibits giant dipole resonances. This vibration process has a resonance frequency at which the absorbed photon excites the nucleus, causing it to emit a neutron, a proton, etc. [19].

Introduction to MCNPX 2.6.0 simulation code

Monte Carlo N-Particle eXtended (MCNPX) is a general-purpose Monte Carlo radiation transport code with three-dimensional geometry and continuous-energy transport of 34 particles and light ions. Since its inception, MCNPX has focused on the needs of the intermediate energy community, here taken to mean incident energies up to a few GeV. The evaluated data libraries are needed to run the code, and several subsidiary libraries are also needed for the physics models in MCNPX. Tracking is done to a user-settable lower kinetic energy cutoff, and particles will decay with their standard half-lives. For neutrons, all reactions given in a particular cross-section evaluation (such as ENDF/B-VI) are accounted for. Thermal neutrons are described by both the free gas and S (alpha, beta) models. For photons, the code accounts for incoherent and coherent scattering, the possibility of fluorescent emission after photoelectric absorption, absorption in pair production with local emission of annihilation radiation, and bremsstrahlung. A continuous slowing-down model is used for electron transport that includes positrons, X-rays, and bremsstrahlung, but does not include external or self-induced fields [20]. MCNPX contains numerous flexible tallies: surface current & flux, volume flux (track length), point or ring detectors, particle heating, fission heating, pulse height tally for energy or charge deposition, mesh tallies, and radiography tallies [21].

When a particle starts from a source, a particle track is created. If that track is split two-for-one at a splitting surface or collision, a second track is created and there are now two tracks from the original source particle, each with half the single-track weight. Within a given cell of fixed composition, the method of sampling a collision along the track is determined by using the following theory: the probability of a first collision for a particle between l and $l + dl$ along its line of flight is given by Eq. (1) [20]:

$$p(l)dl = e^{-\Sigma_t l}\,\Sigma_t\; dl \tag{1}$$

where Σ_t is the macroscopic total cross-section of the medium and is interpreted as the probability per unit length of a collision. Setting ξ the random number on (0,1) to be Eq. (2).

$$\xi = 1 - e^{-\Sigma_t l} \tag{2}$$

It follows that Eq. (3).

$$l = -\frac{1}{\Sigma_t}\ln(\xi) \tag{3}$$

In addition, the cosine of the angle between the incident and exiting particle directions is sampled from angular distribution tables in the collision nuclide's cross-section library [20].

Assumptions of the problem for simulation with MCNPX

As our previous study shows [9], for a typical granite rock with the chemical compound as indicated in Table 1, the piezoelectric coefficient (d) equals 7×10^{-13} C/N (at room temperature),relative permittivity (ϵ_r) equals 5 and uniaxial compressive strength of 140 MPa,when the compressive stress is applied on various sizes of rock block, the atomic/nuclear particles are radiated from the rock medium.

Table 1. Elemental percentage of the granite, based on its chemical composition.

Elements	O	Si	Al	K	Na	Ca	Fe	Total
Percentage, %	62	22.5	9	3	2	0.5	1	100

To find how much the propagated atomic/nuclear particles that is produced from piezoelectric granite rocks deep inside the Earth can reach the surface, we first supposed that the particles have been produced from a hypocenter with a focal depth of 2 km. Such an EQ would be categorized among the shallow EQs.

Then, we assumed that a fracture had been produced as a result of different kinds of EQ stresses (tensional, compressive, or shear stress) on the rock block. Hence, the **cell card** and **surface card** of the code were defined for this fracture as a rectangular shape with depth (d), length (l), and width (w) equal to 2,000 m, 1,000 m, and 10 cm, respectively. The width (w) of the fracture is an affecting parameter on the number of created particles and flux. Hence, we have selected a normal width of 10 cm for a typical fracture. Nevertheless, it can be argued that as the width of the fracture increases, the source and created new particles have fewer interactions with the surrounding rocks, and hence, the flux of the various particles in the upper sections of the fracture will be higher.

In the **material card**, we supposed that the fracture has been filled with air, water, and CO_2. It must be noted that if the fracture is not filled with any kind of material (vacuum occupies the whole volume of the fracture), all particles with the initial energy they have achieved can reach the surface with no capturing and energy loss.

Another input parameter of the code is the **density of the material**. Normally, the fluids beneath the surface are under pressure as a result of their hydrostatic column and also due to the upper formations' weight. However, in the model, proposed by Moore et al. [16], the invaded air into

the fractures possesses a lighter density than the atmospheric air density because of the higher heat at depth. Hence, for those near surface fractures that make pathways to the surface in which the air is not under upper layers' pressure although the hydrostatic column results in higher air density at depth the high temperature at depth has a converse effect and it compensates the rise in the air density. Therefore, we have assumed that the fractures' filling air is not under pressure and we have chosen the air density equal to 1.2041 kg/m^3 at 20 ^{0}C and atmospheric pressure.

For the water, since it is almost an uncompressible fluid, its density at depth does not change considerably in relation to the surface, and thus, we have set its density equal to 1,000 kg/m^3.

For the CO_2, for those near surface fractures that make pathways to the surface, the condition is the same as for the air, and we have chosen its density equal to 1.870 kg/m^3 in the normal temperature and atmospheric condition. However, at EQ hypocenters, CO_2 pressure can reach 10-20 MPa. At a depth of about 20 km, the temperature could rise to about 600 ^{0}C [22]. In this condition, the CO_2 is in a supercritical phase and the density of this gas at 577 ^{0}C and 10 MPa pressure equals 61.31 kg/m^3 [23].

As investigated in our previous research, the initial energy of the runaway electrons inside the granite rock tissues can be calculated, by applying the piezoelectric and elastic energy relationships. The average energy of the created particles can be estimated, using the MCNPX simulation. Table 2 reveals the computed initial energy of the runaway electrons and the estimated average energy of the created particles inside the granite rock tissue, achieved from the simulation outputs in NPS electron = 1000 for two EQ Richter magnitudes (M_L) [9].

Table 2. The computed initial energy of the runaway electrons and the estimated average energy of the created particles inside the granite rock tissue, achieved from the simulation outputs in NPS electron = 1000 for two M_L [9].

Block size (m^3)	M_L	Initial electrons' energy, MeV	The average energy of the created particles (MeV)			
			Neutrons	Photons	Electrons	Protons
400^3	**5.79**	885	10.4	1.81	0.03	9.38
4000^3	**7.67**	8858	24.6	3.05	0.04	20

As can be seen in this table, neutron (n), proton (h), electron (e), and photon (γ) particles are created from the photonuclear and/or other atomic/nuclear interactions of the runaway electron avalanche in piezoelectric rocks being under a huge amount of stress. Besides, although the initial energy of the runaway electrons is too high for these two EQ magnitudes, the average energy of the created electrons is relatively low. That is due to various interactions of runaway electron avalanches inside the rock tissue, especially the "knock on electrons" interactions, resulting in different particle radiation and lowering the average energy of the total created electrons. Thus, in the **source card**, we considered the neutrons, protons, and gammas as the source particles, separately and we neglected the electrons because of their low energy.

The **physics cards** for each of the source particles include some input parameters, set according to the conditions and requirements of the problem. For instance, the parameter *emax* in neutron, proton, and electron physics and the parameter *emcpf* in photon physics indicates the upper limit of the particle's energy.

RESULTS AND DISCUSSION

Simulation when the fracture is filled with air

As already discussed, a deep fracture in the Earth's crust can be filled with air. In this case, for each of the source particles—neutron, proton, and photon we wrote the simulation code for two EQ magnitudes. It must be noted that for simplicity, we have defined the chemical composition of the air as 80 % nitrogen plus 20 % oxygen in our written code, and the other chemical compounds of the air, containing very little percentage were eliminated.

Table 3 represents the input parameters for the simulation of the neutron propagation inside an air-filled fracture when an EQ with M_L = 7.67 occurs inside a granite block. The average energy for each source particle was achieved from the Table 2. In addition, the number of particles (NPS) in the written code was supposed to be 100'000, since, that is enough to achieve the appropriate results. The simulation running time (CTME) was about 106 min.

When 24.6 MeV neutrons, already created as a result of the piezoelectric effect, are propagated into an air-filled fracture and have interactions with atoms of the air and the surrounded granite rock, various atomic/nuclear interactions would be anticipated and some new particles will be generated. Some of the particles, by their elastic or inelastic interactions with surrounding granite atoms/nuclei, will be recoiled into the air.

Table 3. Input parameters for simulation of the neutron propagation inside an air-filled fracture when an EQ with M_L= 7.67 occurs inside a granite block.

M_L	material	fracture dimensions, m^3	source particle	average energy (MeV)	source position	source direction	No. of particles (NPS)
7.67	air	2000×1000×0.1	n	24.6	bottom surface	bottom to top surface	100'000

To achieve a model of the created particle flux, the fracture cell was divided into 125'000 meshes with the rectangular mesh tally card (RMESH) of the MCNPX. The type I of this mesh tally was employed. Since the output of this card is a binary file, we used the *gridconv* program to convert it to a data file (*.dat). Then, we applied the *Tecplot* software to plot the 2D view of the constructed mesh tally and the amount of particle flux in the unit of No. /cm^2/s per each source particle (to find the real flux amount, the flux, shown in the mesh tally must be multiplied by the NPS number).

It must be taken into account that *Tecplot* software did not plot the simulation results near the width's left and right boundaries of the hypothesized fracture in 2D views. Therefore, the output images were shown for only the middle 5 cm of the width of the fracture in all figures.

Fig. 1 indicate the 2D views of neutron, electron, photon, and proton fluxes per each source particle in an air-filled fracture when the source particle is neutron with E_n = 24.6 and 10.4 MeV (for EQs with M_L = 7.67 and 5.79, respectively).

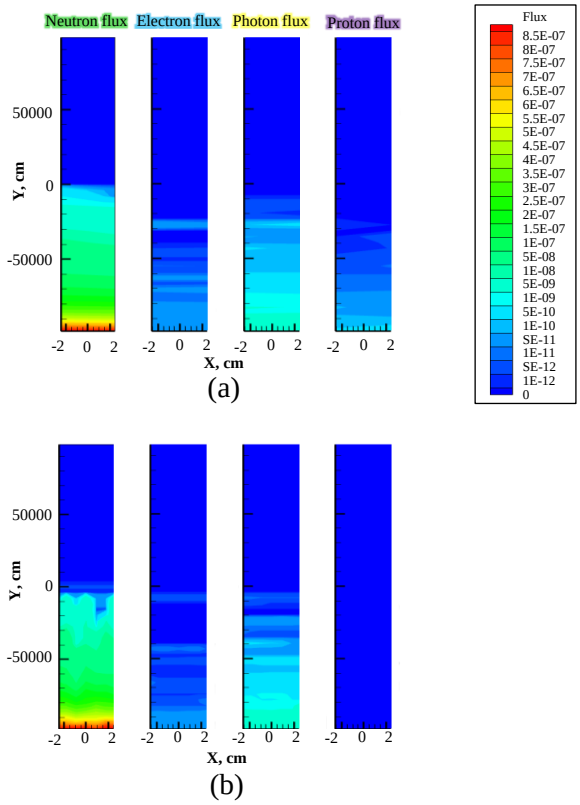

Fig. 1. 2D views of neutron, electron, photon, and proton fluxes per each source particle in an air-filled fracture when the source particle is neutron with (a) E_n = 24.6 MeV and (b) E_n = 10. 4 MeV (for EQs with M_L = 7.67 and 5.79, respectively).

As is evident in this figure, for E_n = 24.6 MeV, we would expect the flux of neutrons to be almost up to 1 km above the source position and after that, all created neutrons inside the air are lost (captured or their energy decreased below the cut-off energy). However, for E_n= 10.4 MeV, the flux up to 950 m above the source position would be expected. For E_n = 24.6 and 10.4 MeV, we would also expect the electron flux up to about 780 and 950 m, photon flux up to about 900 and 950 m, and proton flux up to about 800 and 0 m, respectively.

In addition, Table 4 illustrates the simulation results for some of the created particles' characteristics, including "number", "average energy", "mean free path (*mfp*)" and "average time of capture or escape" in an air-filled fracture when the source particle is neutron, photon, and proton with NPS=100'000 and the energies equivalent to M_L= 7.67 and 5.79, respectively. As could be found in this table, when the source particle is neutron with E_n = 24.6 MeV (equivalent to M_L= 7.67), the *mfp* of created new neutrons and photons in the air are 133 and 158 m, respectively. In comparison, when the source neutron possesses energy equal to 10.4 MeV (equivalent to M_L= 5.79), the *mfp* of created neutrons and photons in the air are 141 and 181 m, respectively, representing the higher value, because of lower interactions (lower cross sections) of these particles with the air's atoms/nuclei. The *mfp* for created electrons and protons are much lower (in cm dimension) due to their Coulomb interactions with the other atoms/nuclei. Besides, when the source neutron contains the energy equal to 24.6 MeV, the average time of capture or escape for created neutrons and photons are 2.68E-04 and 1.87E-04, respectively, and for electrons and protons, this could not be calculated by the MCNPX due to their very prompt capture or escape in/from the environment.

Table 4. The simulation results for some of the created particles' characteristics, in an air-filled fracture when the source particle is neutron, photon, and proton with NPS=100'000 and the energies equivalent to M_L= 7.67 and 5.79 MeV, respectively.

NPS=100'000				Created particles' characteristics				
Fracture filling material	M_L	Source particle	Source particle's Energy, MeV	Particles	No.	Average energy, MeV	Mean free path (*mfp*), cm	Average time of capture or escape, s
air	7.67	neutron	24.6	neutron	112686	2.31E+01	1.33E+04	2.68E-04
				electron	94389550	1.59E-02	2.05E+01	…..
				photon	1207243	9.24E-01	1.58E+04	1.87E-04
				proton	42362	5.07E+00	3.65E+00	…..
air	7.67	photon	3.05	neutron	0	0.00E+00	0.00E+00	0
				electron	27029959	1.56E-02	2.45E+01	…..
				photon	329562	9.49E-01	2.34E+04	7.60E-07
				proton	0	0.00E+00	0.00E+00	….
air	7.67	proton	20	neutron	31	3.49E+00	8.34E+03	3.35E-04
				electron	250243	1.59E-02	9.24E+00	…..
				photon	3098	9.53E-01	1.86E+04	3.48E-05
				proton	100783	1.99E+01	1.26E+01	…..
air	5.79	neutron	10.4	neutron	100000	1.04E+01	1.41E+04	2.21E-04
				electron	75862285	1.60E-02	2.10E+01	…..
				photon	965231	9.31E-01	1.81E+04	1.90E-04
				proton	6366	3.49E+00	6.94E-01	…..
air	5.79	photon	1.81	neutron	0	0.00E+00	0.00E+00	0
				electron	16646303	1.47E-02	1.36E+01	…..
				photon	132001	7.88E-01	1.77E+04	5.75E-07
				proton	0	0.00E+00	0.00E+00	….
air	5.79	proton	9.38	neutron	0	0.00E+00	0.00E+00	0.00E+00
				electron	30057	1.53E-02	6.09E+00	…..
				photon	386	8.89E-01	1.58E+04	1.22E-08
				proton	105	9.37E+00	2.88E+00	…..

Furthermore, Fig. 2 indicate 2D views of neutron, electron, photon, and proton fluxes per each source particle in an air-filled fracture when the source particle is the photon with E_γ = 3.05 and 1.81 MeV (for EQs with M_L = 7.67 and 5.79, respectively). As can be understood from this figure, for E_γ = 3.05 MeV, we would expect the flux of photons, almost equal to 1E-8 γ/cm^2/s about 1.6 km above the source position (EQ hypocenter), and after that, almost all created photons inside the air are lost. However, for E_γ = 1.81 MeV, the same flux at about 1.2 km above the source position would be expected. We would also expect the flux of electrons up to about 1.7 and 1.4 km for E_γ = 3.05 and 1.81 MeV, respectively. The neutron and proton fluxes are almost zero along the whole fracture length, because, the source photons' energy is not high enough to initiate the photonuclear interactions.

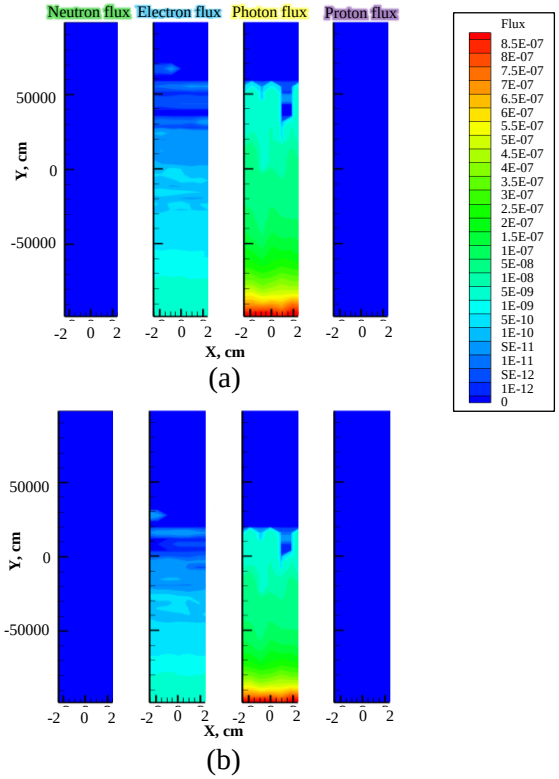

Fig. 2. 2D views of neutron, electron, photon, and proton fluxes per each source particle in an air-filled fracture when the source particle is the photon with (a) E_γ = 3.05 MeV and (b) E_γ = 1.81 MeV (for EQs with M_L = 7.67 and 5.79, respectively).

Figs. 3 and 4 illustrate the photonuclear total cross section versus the photon energy in ^{14}N and ^{16}O (the main constituent parts of the air), plotted from ENDF library of nuclear data services web page [24]. As can be seen in these figures, the photonuclear interaction in ^{14}N and ^{16}O initiates at 7.55 MeV and 12.5 MeV, respectively. These energies are higher than 3.05 and 1.81 MeV (the average photon's energy, released from the EQs with M_L= 7.67 and 5.79 in granite block, respectively), and hence, no neutrons nor protons are released from photonuclear reactions of the air atoms' nuclei.

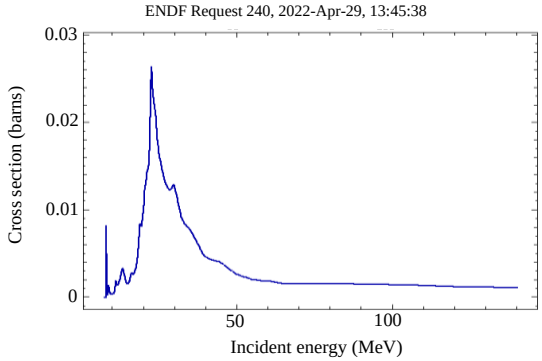

Fig. 3. The photonuclear total cross section versus the photon energy in ^{14}N, plotted from ENDF library data.

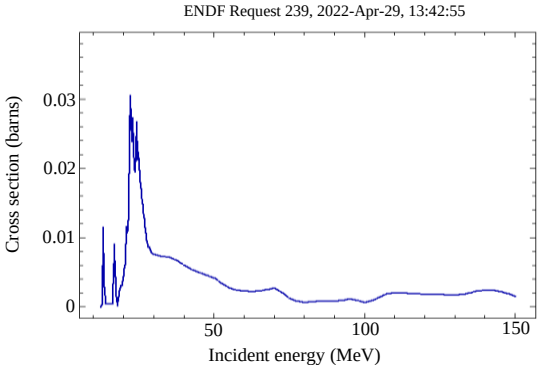

Fig. 4. The photonuclear total cross section versus the photon energy in ^{16}O, plotted from ENDF library data.

It must be taken into consideration that, since the photon has a wave-particle duality, whenever it possesses low energy, its frequency is low enough to allow the electromagnetic wave to pass through kilometers of solids. Therefore, ultra-low frequency (ULF) photon waves can reach themselves to the surface via empty or gas-filled fractures or even solid rocks.

Moreover, Fig. 5 reveal 2D views of neutron, electron, photon, and proton fluxes per each source particle in an air-filled fracture when the source particle is the proton with E_h = 20 and 9.38 MeV (for EQs with M_L = 7.67 and 5.79, respectively). As could be seen in this figure, for both E_h = 20 and 9.38 MeV, the protons have a flux of 5E-12 h/cm^2/s up to about 50 m above the hypocenter (source position) and then, they are all lost. Besides, very little flux of photons and electrons up to about 50 m from the hypocenter and almost no neutron flux can be anticipated.

The reason for very little particle creation and flux when the source particles are protons could be the fact that, the protons have normally short mean free path (*mfp*) in relation to the neutrons because of their electric charge (Coulomb interactions). Once they are created, they will have atomic or nuclear interactions (elastic, inelastic, fusion, etc), promptly. They might also create stable hydrogen atoms by attracting electrons.

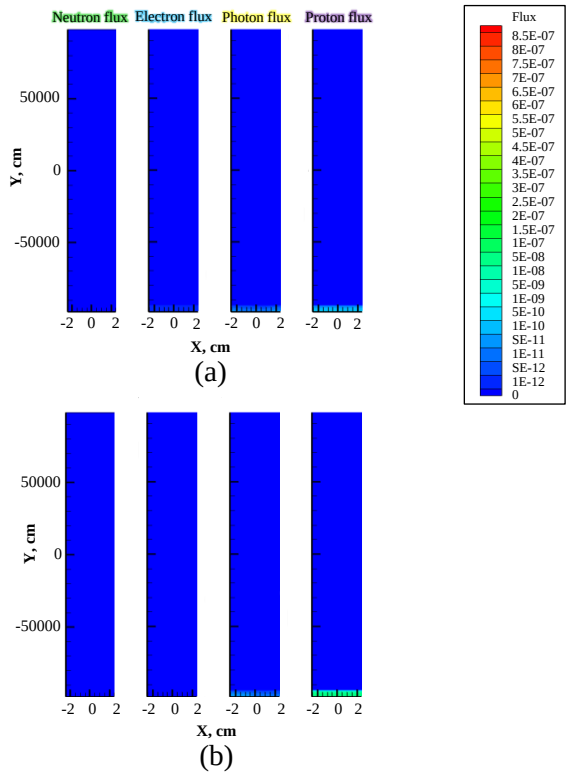

Fig. 5. 2D views of the neutron, electron, photon, and proton fluxes per each source particle in an air-filled fracture when the source particle is the proton with (a) E_h = 20 MeV and (b) E_h = 9.38 MeV (for EQs with M_L = 7.67 and 5.79, respectively).

Simulation when the fracture is filled with water

We also wrote the same simulation code when the fracture was filled with water (the water's chemical composition and density were given to the code). Table 5 represents the input parameters for the simulation of the neutron propagation inside a water-filled fracture when an EQ with M_L= 7.67 happens inside a granite block. The simulation running time (CTME) was about 63 min.

Table 5. Input parameters for simulation of the neutron propagation inside a water-filled fracture when an EQ with M_L= 7.67 is happened inside a granite block.

M_L	material	fracture dimensions, m^3	source particle	average energy (MeV)	source position	source direction	No. of particles (NPS)
7.67	water	2000×1000×0.1	n	24.6	bottom surface	bottom to top surface	100'000

Fig. 6 represent 2D views of different particle fluxes per each source particle in a water-filled fracture when the source particle is neutron with E_n= 24.6 MeV, photon with E_γ= 3.05 MeV; and proton with E_h= 20 MeV, respectively (all for EQ of the M_L = 7.67). As is evident in this figure, in all situations, the flux of particles can be seen up to about 50 m above the source position and then, almost all created particles inside the water are lost (captured or their energy is reduced below the cut-off energy).

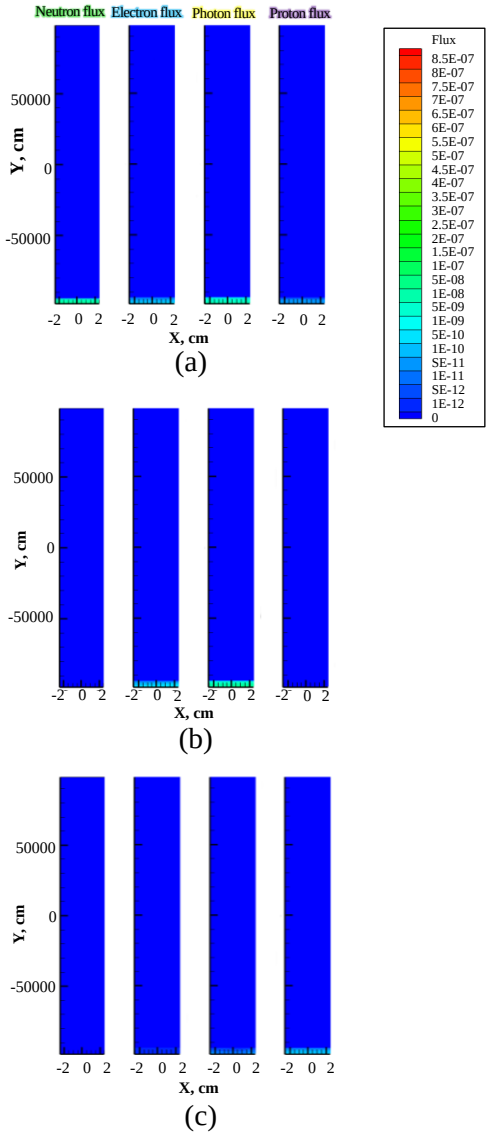

Fig. 6. 2D views of different particle fluxes per each source particle in a water-filled fracture when the source particle is (a) neutron with E= 24.6 MeV, (b) photon with E= 3.05 MeV, and (c) proton with E= 20 MeV (all for EQ with ML = 7.67).

The water density, being much higher than the air density, is the most affecting parameter, resulting in particles' capturing or lowering their energy below the cut-off energy. Therefore, it can be argued that if the fractures around the EQ's hypocenter are filled with water, the radiated particles from the piezoelectric mechanism cannot be transmitted to a long distance or the surface of the Earth even if the EQ magnitude is high.

Simulation when the fracture is filled with CO_2

We also wrote the simulation code with the same parameters when the fracture is filled with CO_2. However, for its density, as previously explained in section 2.2, we have chosen its density equal to 1.870 kg/m^3 in the normal pressure/ temperature condition. Nevertheless, since at depths below 20 km, CO_2 pressure and temperature are

much higher, for comparison, we have also applied the density equals 61.31 kg/m^3 for the pressure at 10 MPa and temperature at 577 ^{0}C.

Fig. 7 represent 2D views of neutron, electron, photon, and proton fluxes per each source particle in a CO_2-filled fracture when the source particle is the photon with E_γ = 3.05 MeV (for EQ with M_L = 7.67) and the density of CO_2 is 1.870 and 61.31 kg/m^3, respectively.

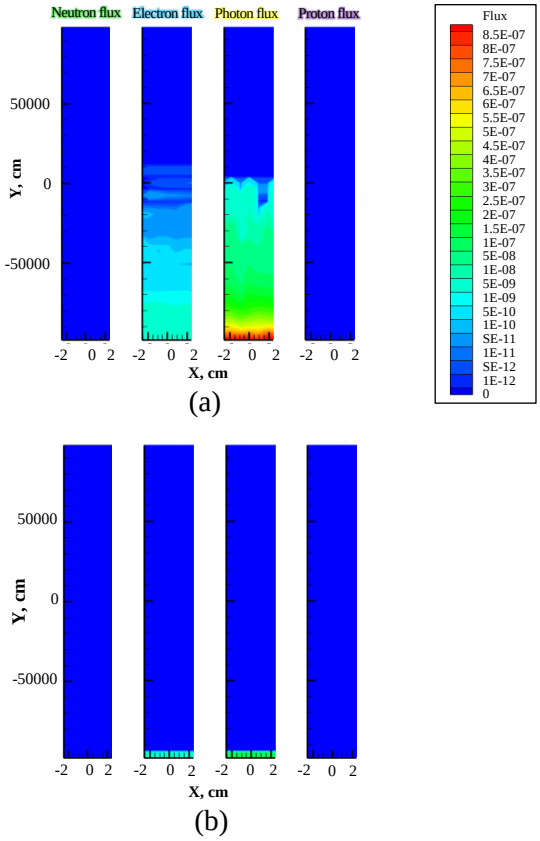

Fig. 7. 2D views of neutron, electron, photon, and proton fluxes per each source particle in a CO_2-filled fracture when the source particle is neutron with E_γ = 3.05 MeV (for EQ with M_L = 7.67) and the density of CO_2 is (a) 1.870 kg/m^3 and (b) 61.31 kg/m^3, respectively.

As understood from this figure, when the CO_2 density is 1.870 kg/m^3, we can expect the flux of photons and electrons far from the source position (more than a kilometer). In comparison, when the CO_2 density is 61.31 kg/m^3, the flux of particles, about 50 m above the source position reduces rapidly, and thereafter, almost all created particles inside the CO_2 are lost (captured or their energy is reduced below the cut-off energy).

CONCLUSION

We estimated the flux of the particles inside an assumed rectangular-shaped fracture, filled with air, water, and CO_2 at different distances from the EQ hypocenter using the MCNPX simulation code. Those particles are created from under-stressed piezoelectric rocks and also from the interactions between them and the filling fluid's atoms/nuclei. It was found that inside a water-filled fracture, the particles do not show the flux far from the EQ hypocenter even if the EQ magnitude is high (more than 7 in Richter's magnitude). Nonetheless, inside the fractures, filled with gases like air and CO_2 with lower density that could be expected when the EQ hypocenter is very shallow (0–5 km), various types of particles can have a flux far from the source (more than a kilometer) and they might reach themselves to the surface. However, for deep EQs, it seems that the most detected atomic/ nuclear particles on the surface have been transmitted via vacuum-filled fractures. If the radiated stable particles like electrons or photons move alongside and parallel to the fracture walls, they can pass long distances from the EQ hypocenter inside the vacuum without any interactions with the surrounding rocks and reach themselves to the surface even with their initial energy.

In addition, by running the simulation code on a CO_2-filled fracture, it was concluded that the higher the density of the fracture's filling fluid, the less distance that the particles will show a flux.

Moreover, it was found that the type and density of the filling fluid, the fracture's geometry and size, especially the width of the fracture and, the moving direction of the source particles are among the important factors, affecting how much the particles can reach themselves to the surface.

It must be taken into account that we have considered the "average energy" of the created particles (as source particles in the EQ hypocenter) from various atomic/nuclear interactions due to the piezoelectric effect for each EQ magnitude. However, our previous study reveals that in some interactions, the generated particles obtain higher energies than the average, and hence, those particles can represent higher flux through a fluid-filled fracture.

ACKNOWLEDGMENT

We would like to thank the Payame Noor University for preparing a qualified environment to perform this research project.

AUTHOR CONTRIBUTION

A. Bahari: idea expanding, writing, editing, corresponding author; S. Mohammadi: supervision, verification; N. Shayan Shakib, M. R. Benam, Z. Sajjadi: Co-advisor and verification.

REFERENCES

1. X. Guo, J. Yan and Q.Wang, J. Environ. Radioact. **213** (2020) 106119.
2. N. Salikhov, A. Shepetov, G. Pak *et al.*, Atmos. **14** (2022) 1667.
3. C. Tsabaris, J. Radioanal. Nucl. Chem. **330** (2021) 755.
4. A. U. Maksudov and M. A. Zufarov, Earthquake Sci. **30** (2017) 283.
5. Y. Stenkin, V. Alekseenko, Z. Cai *et al.*, J. Environ. Radioact. **208-209** (2019) 105981.
6. P. Picozza, L. Conti and A. Sotgiu, Front. Earth Sci. **9** (2021) 676775.
7. M. R. M. Daneshvar and F. T. Freund, Swiss J. Geosci. **112** (2019) 435.
8. A. Carpinteri and G. Niccolini, Sci. **1** (2019) 17.
9. A. Bahari, S. Mohammadi, M. R. Benam *et al.*, Radiat. Eff. Defects Solids **177** (2022) 743.
10. D. Mindaleva, M. Uno and N. Tsuchiya, Geophys. Res. Lett. **50** (2023) e2022GL099892.
11. E. Warren-Smith, B. Fry, L. Wallace *et al.*, Nat. Geosci. **12** (2019) 475.
12. K.Ujiie, H.Saishu, A. Fagereng *et al.* Geophys. Res. Lett. **45** (2018) 5371.
13. J. Nakajima and N. Uchida, Nat. Geosci. **11** (2018) 351.
14. Y. Mukuhira, M. Uno and K. Yoshida, Commun. Earth Environ. **3** (2022) 286.
15. J. G. Berryman, Geophys. J. Int. **171** (2007) 954.
16. J. R. Moore, V. Gischig, M. Katterbach *et al.*, Earth Surf. Processes Landforms **36** (2011) 1985.
17. I. B. Vodopiyanov, J. R. Dwyer, E. S. Cramer *et el.*, J. Geophys. Res.: Space Phys. **120** (2015) 800.
18. D. Sarria, C. Rutjes, G. Diniz *et al.* Geosci. Model Dev. **11** (2018) 4515.
19. E. M. A. Hussein, Radiation Mechanics, Principles and Practice, 1st ed., Elsevier Science, Oxford (2007) 153.
20. L. S. Waters, G. W. McKinney, J. W. Durkee *et al.*, AIP Conf. Proc. **896** (2007) 81.
21. Los Alamos National Laboratory, Monte Carlo Methods, Codes, & Applications Group. https://mcnp.lanl.gov/. Retrieved in March (2023).
22. S. A. Miller, C. Collettini, L. Chiaraluce *et al.*, Nat. **427** (2004) 724.
23. Anonymous, Engineering ToolBox, Carbon dioxide - Density and Specific Weight vs. Temperature and Pressure. https://www.engineeringtoolbox.com/carbon-dioxide-density-specific-weight-temperature-pressure-d_2018.html, Retrieved in March (2023).
24. International Atomic Energy Agency (IAEA), Evaluated Nuclear Data File (ENDF). https://www-nds.iaea.org/exfor/endf.htm. Retrieved in March (2023).